energies

MDPI

Article

Aerodynamic Study on the Influence Mechanism of Bow Blades on the Flow Field of Supersonic Tandem Rotors

Hao Cheng, Zhaoyun Song and Bo Liu *

School of Power and Energy, Northwestern Polytechnical University, Xi'an 710072, China; chenghao144@sina.com (H.C.); songzhaoyun@mail.nwpu.edu.cn (Z.S.)
* Correspondence: liubo704@nwpu.edu.cn

Abstract: In order to research the influence mechanism of bow blades on the flow field of supersonic tandem rotors of compressors, the supersonic rotor rotor37 is taken as the prototype and redesigned as a supersonic tandem rotor. Compared with the prototype rotor37, the efficiency of the design tandem rotor is increased by 0.24% and the stall margin is increased by about 5.6%. Although the negative bow blade deteriorates the flow field in the tip region and the hub region, it significantly increases the efficiency and total pressure ratio of the tandem rotor from 20% span to 85% span. The efficiency of the design point of the tandem rotor with a negative bow angle of 10° is improved by 0.37%, and the stall margin is also increased to 20.71%. Positive bow blades improve the efficiency of the hub region and casing region of tandem rotors, but they significantly reduce the efficiency of the tandem rotor from 10% to 50%. The positive bow blade reduces the pressure ratio and efficiency at the design point and reduces the stall margin of the tandem rotor. The design point efficiency of the tandem rotor with a positive bow angle of 10° is decreased by 0.3%, the stall margin is decreased by 1%, and the mass flow of the design point is increased by 0.38%.

Keywords: compressors; supersonic tandem rotors; the stall margin; positive bow blades; negative bow blades; the hub region and casing region

Citation: Cheng, H.; Song, Z.; Liu, B. Aerodynamic Study on the Influence Mechanism of Bow Blades on the Flow Field of Supersonic Tandem Rotors. *Energies* **2022**, *15*, 4474. https://doi.org/10.3390/en15124474

Academic Editor: Valery Okulov

Received: 12 April 2022
Accepted: 14 June 2022
Published: 20 June 2022

1. Introduction

A high blade Mach number and severe three-dimensional flow effects are the main characteristics of transonic high-load compressors, which increase the high-intensity shock losses and secondary flow losses of transonic compressors. Bow blades and sweep blades have been widely used in the aerodynamic design of high-load fans and compressors as effective means to improve the three-dimensional shock wave structure of the rotor and reduce the secondary flow loss of transonic compressors [1–4]. Blaha et al., Denton et al., and Bergner et al. [5–8] proved that a rotor forward sweep can improve the three-dimensional structure of rotor shock waves, improve the flow field at rotor tip, weaken the tip shock loss and the interaction loss between shock waves and boundary layer, and improve compressor performance and stability margin.

Hah et al. and Wadia et al. [9,10] found that sweep blades can increase the peak efficiency of the rotor, but may reduce the stable operating range. Cao et al. [11] conducted research on the effect of bow blades on the performance of the transonic compressor rotor and the interaction between shock wave and tip leakage flow. It was found that the positive-bow of the blade (bow to the blade pressure surface) reduces the efficiency of the transonic rotor. For the negative-bow rotor, with the increase of the negative-bow angle, the peak efficiency and the total pressure ratio shows a trend of first increasing and then decreasing. Razavi et al. [12] carried out the three-dimensional optimized design of sweep and bow transonic rotors to achieve maximum stage pressure ratio, efficiency, and operating range. The results show that the optimized three-dimensional blade can increase the working range by 30%, the pressure ratio by 1%, and the efficiency by 2%. The above research

results show that the bow blade can reduce the shock wave intensity, weaken the loss of the shock wave and the boundary layer, and improve the aerodynamic performance of the compressor.

The research of high load transonic compressors is of great significance for aero-engine weight reduction and thrust-to-weight ratio improvement. Compared with a single blade, a tandem blade has the advantages of small loss and large flow turning angle, mainly because the deceleration and expansion of air flow are realized on the front blade and aft blade, respectively. Therefore, a tandem blade is considered to be an effective means to improve compressor loads. Researchers at home and abroad have carried out some studies on the tandem blade. Bammert et al. [13–15] studied the application of tandem rotors in multistage axial flow compressors, and the results showed that flow loss of tandem blades was about 18% lower than that of conventional blades. Based on experiment results, Wu et al. [16] and Roy and Saha et al. [17,18] found that axial overlap (AO) and pitch proportion (PP) had a great influence on the flow and performance of tandem blades. The optimal axial overlap was distributed in the interval [−0.1, 0], and the interval of optimal pitch proportion was [0.8, 0.9]. Urasek et al. [19] designed and tested a transonic tandem rotor, nd the tandem rotor has a design pressure ratio of 1.77, adiabatic efficiency of 88%, and stall margin of 10%. Hasegawa et al. [20] studied the design of transonic tandem fans and finished the design and test of a high-pressure ratio transonic fan. The structure of the fan is composed of an inlet guide vane, rotor, stator, and outlet guide vane. The isentropy efficiency of the fan is 0.80, the pressure ratio is 2.2, and the stall margin is about 10%. The tandem compressor designed by Sakai et al. [21] has an adiabatic efficiency of 84.9%, a pressure ratio of 2.3, and a stall margin of about 10%. McGlumphy et al. have applied tandem rotor technology at the high pressure compressor outlet with a design point load factor of 0.54, adiabatic efficiency of 0.91, and stall margin of 19%. The results show that tandem rotors have significant advantages in load capacity and efficiency compared to individual rotors at subsonic conditions [22,23].

Since the tandem blade was proposed, it has been of great concern to researchers due to its high load and high efficiency. However, due to the serious interference between the front and aft blade of the tandem blade, the three-dimensional flow characteristics of the tandem blade are more complex than those of conventional single blade. Therefore, it is of great significance to use flow control technology to reduce the influence of strong three-dimensional flow characteristics on tandem blades.

Most of the open literature studied the application of bow blades and sweep blades in transonic compressor rotors, and the research about the influence mechanism of bow blades on the flow of supersonic tandem rotors is rare. In order to explore the influence mechanism of bow blades on flow fields and shock wave strength and position of the tandem blade, this paper carried out some relevant research on supersonic tandem rotors. The main contribution of this study is two-fold. The supersonic rotor Rotor37 is taken as the prototype, and the first contribution is to finish a supersonic tandem rotor design. Based on the tandem rotor, the second goal is to study the influence of different bow blades on the flow field structure of the supersonic tandem rotor in detail.

2. Numerical Method and Validation

In this paper, the commercial software NUMECA is used for CFD numerical simulation to solve the three-dimensional Reynolds average RANS equation in the form of finite volume. The Spalart–Allmaras turbulence model is used as the turbulence model. The solid surface adopts non-slip and adiabatic boundary conditions. Total temperature (288.15 K) and total pressure (101,325 Pa) remained unchanged at the inlet, and an average static pressure is specified at the outlet. The grid generation is completed by a NEMECA/AutoGrid5 grid module. An O4H structure grid is used for the single blade, and the tandem blade grid is periodically matched and connected by the O4H grid of front and aft blades to ensure the orthogonality of the grid > 10°. In order to meet the requirement of the Spalart–Allmaras turbulence model where the boundary layer Y+ is less than 10, the grid scale of the near

wall surface is set as 1×10^{-6} m. The numerical simulation calculation domain is formed by extending the inlet and outlet of the blade by 1.5 times the axial chord to ensure the accuracy of the numerical simulation.

In order to verify the accuracy of the numerical simulation method in predicting the performance of the supersonic compressor and capturing the flow field structure, this paper selects the rotor37 with experimental data as the validation object. Table 1 gives the design parameters of rotor37.

Table 1. The design parameters of rotor37.

Parameters	Parameters
Rotating Speed/(r/min)	17,188
Blade number	36
Pressure ratio	2.106
Hub-Tip radius ratio	0.7
Tip clearance/m	0.00036
Flow rate/(kg/s)	20.19

In this paper, a comparative study of the numerical simulation results and experimental results of rotor37 is carried out. Figure 1 shows the comparison between the numerical simulation results and the experimental results under the design speed of rotor37 [24,25]. It is found that the change trend of the characteristic curve of the numerical model is basically consistent with the test results. The highest efficiency obtained by the numerical simulation in this paper is 87.07%, and the corresponding pressure ratio is 2.036. The highest efficiency of the test is 87.6%, the corresponding pressure ratio is 2.056, the efficiency difference between the numerical and test results is 0.5%, the pressure ratio difference is 0.3%, and the differences are within a reasonable range. Figure 2 shows the comparison between the experimental results and the numerical simulation results of the relative Mach number contour of the rotor37 at 95% of the blade height under the peak efficiency point. It shows that the results of the numerical simulation method in this paper are credible.

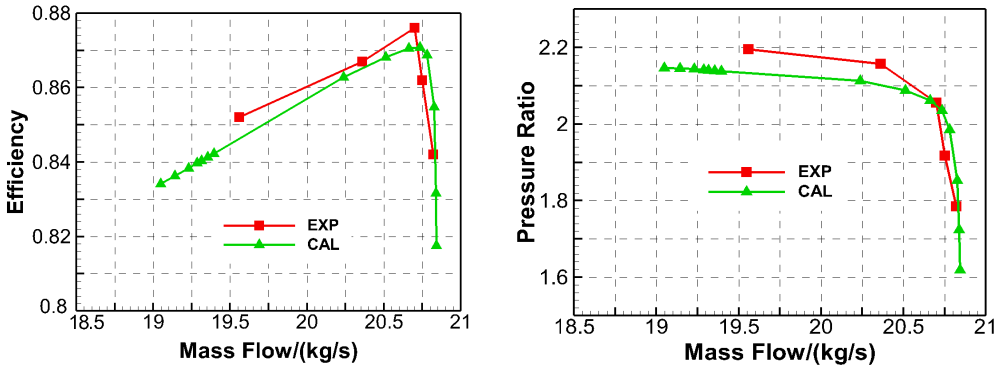

Figure 1. The comparison of the numerical simulation and the experimental results of rotor37. (**a**) the isentropic efficiency. (**b**) the total pressure ratio.

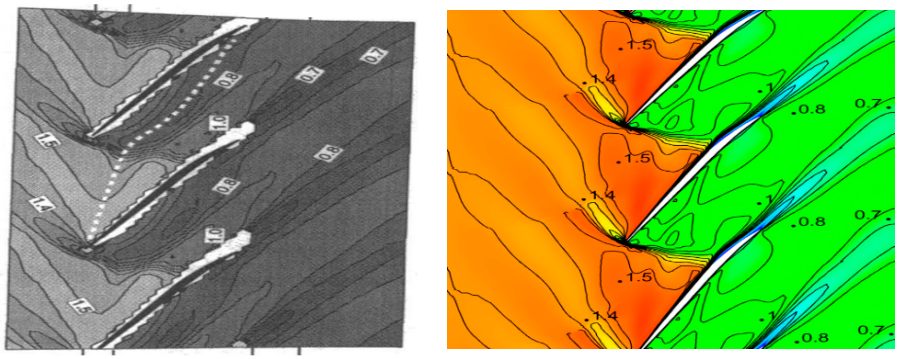

(**a**) (**b**)

Figure 2. The comparison of the relative Mach number at 95% span of the maximum efficiency point. (**a**) the experimental results [25]. (**b**) the numerical simulation results.

3. Design and Analysis of the Original Supersonic Tandem Rotor

In this paper, the supersonic rotor37 is used as the prototype, according to the design scheme of the supersonic tandem blade. In addition, five important design parameters of the tandem rotor are selected, and the tandem modification design of the supersonic rotor37 is carried out. Considering the high Mach number in the middle and tip section of rotor blade, the pre-compression design is used for both the middle and tip blade to reduce the Mach number and shock loss. Figure 3 shows the computational grid for rotor37 and the original tandem rotors (ORG).

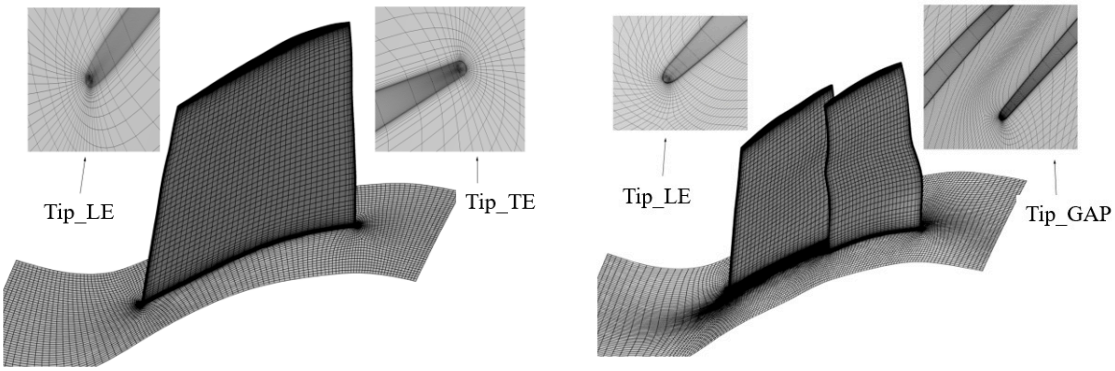

(**a**) (**b**)

Figure 3. The final computational grid of rotor37 and the original tandem rotor. (**a**) rotor37. (**b**) the original tandem rotor.

Figure 4 shows the comparison of the characteristics of rotor37 and the tandem rotor at the design speed. Table 2 shows the comparison of the design point performance and stall margin of rotor37 and the tandem rotor. This paper selects the peak efficiency point as the design point of the rotor. It can be seen that compared with the prototype rotor37, the total pressure ratio of tandem rotor is increased by 0.06, and the efficiency of the tandem rotor increases by 0.24 percentage. The stall margin of the tandem rotor has increased a lot, about 5.6 %, and the definition of the rotor stall margin (*SM*) in this paper is shown in Equation (1). The definition of the isentropic efficiency (η) is shown in Equation (2), and the definition of the static pressure coefficient is shown in Equation (3).

$$SM = \left(\frac{\pi_{stall} * m_{design}}{\pi_{design} * m_{stall}} - 1 \right) * 100\% \quad (1)$$

$$\eta = \frac{(\pi)^{(k-1)/k} - 1}{(T_2/T_1) - 1} \tag{2}$$

$$C_p = \frac{P}{P^*} \tag{3}$$

m_{design}—mass flow of design point
m_{stall}—mass flow near stall point
π_{design}—total pressure ratio of design point
π_{stall}—total pressure ratio near stall point
T_1 and T_2—the total temperature of the compressor inlet and outlet.

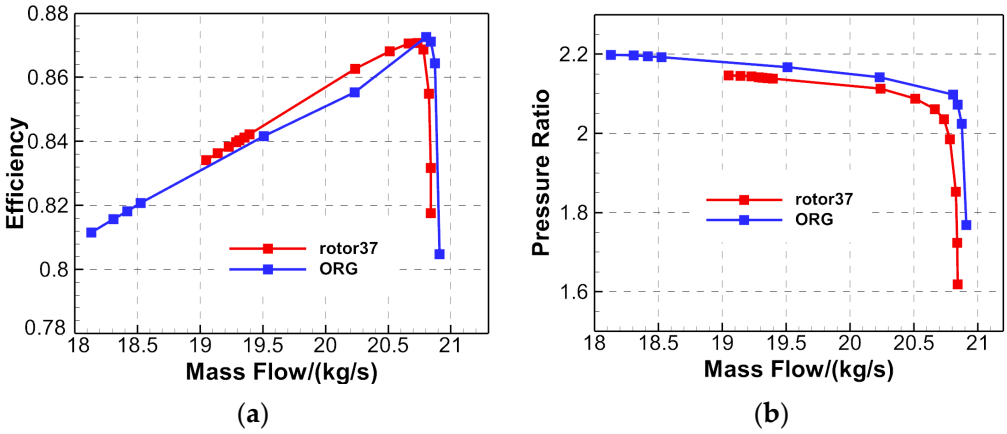

(**a**) (**b**)

Figure 4. The characteristic comparison of rotor37 and the original tandem rotor. (**a**) the isentropic efficiency. (**b**) the total pressure ratio.

Table 2. Comparison of the design point performance and stall margin of rotor37 and the tandem rotor.

Parameters	Mass Flow (kg/s)	Pressure Ratio	Efficiency (%)	Stall Margin
rotor37	20.73	2.036	87.07	14.76%
ORG	20.80	2.098	87.31	20.35%

Figure 5 shows the meridian view and entropy distribution of the design point of rotor37 and the original tandem rotor. Under the same axial chord length, the total pressure loss in the blade tip region of the tandem rotor is obviously smaller than that of the prototype rotor.

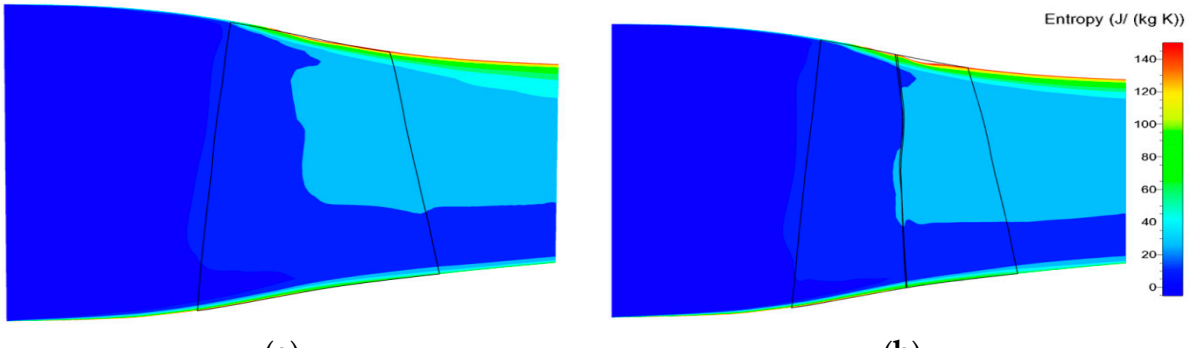

(**a**) (**b**)

Figure 5. The meridian view and entropy distribution of rotor37 and the original tandem rotor. (**a**) the rotor37. (**b**) the tandem rotor.

4. Influence of Bow Blade on Supersonic Tandem Rotors

According to the published relevant literatures [11], the bow blade can change the distribution of pressure of the blade channel along the blade height, so that the low-energy fluid at the end wall migrates to the middle span of the blade. Thereafter, the bow blade can reduce the separation loss of the end wall boundary layer. This paper explores the use of a bow blade to further improve the performance of the designed supersonic tandem rotor, and studies the influence mechanism of bow blades on the flow field of the supersonic tandem rotors.

Figure 6 shows the design method of the bow blade and the computational meshes of the two types of bow tandem blades. As shown in Figure 6a, the bow blade adopted in this paper consists of two second-order Bezier curves of the end wall and a straight line in the middle span of the blade. The control parameters of the bow blade include: the angle of the two end wall curves $(\alpha 1,\ \alpha 3)$, the angle of the middle straight segment $(\alpha 2)$, the spanwise ratio of the two end wall curves $(C1,\ C2)$, and the radial height of the second control point of the end wall two curves $(P1,\ P2)$. The design method of bow blade has many control parameters, and can flexibly apply different bow blade formations to the blade hub section, the blade middle section, and the blade tip section.

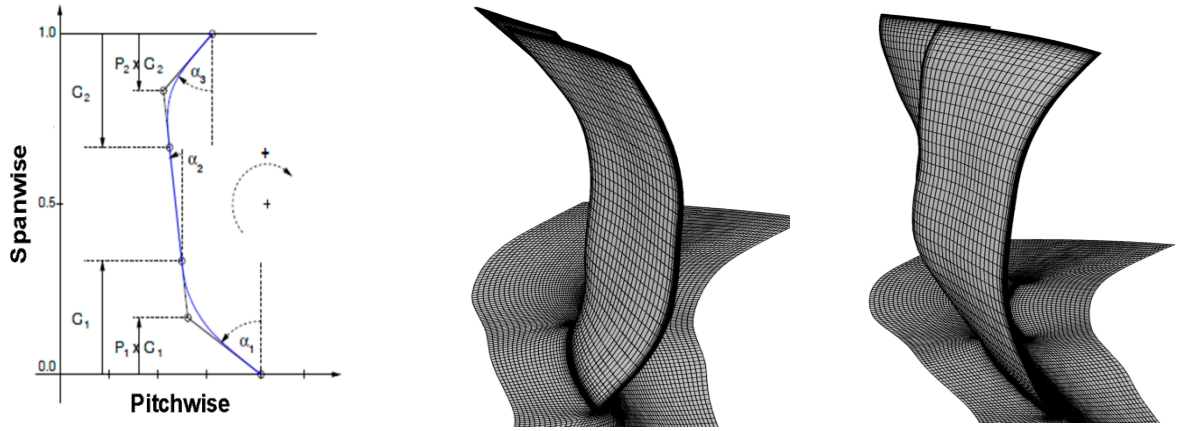

(**a**) (**b**) (**c**)

Figure 6. Design method of bow blade and computational grids of two kinds of bow blades. (**a**) design method of bow blade. (**b**) positive blade at 30°. (**c**) negative blade at 30°.

Considering that this paper mainly studies the influence of different forms of bow blades on the flow field structure of supersonic tandem blades, the design method of bow blades is simplified, and the angle of the middle straight section is taken as 0°. The spanwise ratio and the angle of the two curves of the end wall are equal, and the position of the second control point of the two curves of the end wall is the midpoint of the curve. The design parameters of the simplified bow blade are composed of two control parameters: the bow angle of the end wall curve and the spanwise ratio of the end wall curve. For the convenience of research, when taking the spanwise ratio of the two curves of the end wall, the bow height is 0.4. In this paper, three kinds of positive bow blades (bow to the suction surface of the blade) and three kinds of negative bow blades (bow to the pressure surface of the blade) are studied, respectively, to find out the influence on the flow field structure of supersonic tandem blades with different bow angles. The bow angle corresponding to three positive bow blades and three negative bow blades is 10°, 20°, and 30°, respectively. For the convenience of description, PB10, PB20, PB30 and NB10, NB20, NB30 are used to represent the three positive bow blades and the three negative bow blades, respectively.

4.1. Influence of a Negative Bow Blade on Supersonic Tandem Rotors

Figure 7 shows the comparison of isentropic efficiency and total pressure ratio characteristics of NB10, NB20, and NB30, and Table 3 shows the comparison of design point performance and the stall margin of NB10, NB20, and NB30. It can be seen that, compared with the original tandem rotor (ORG), the negative bow blade increases the pressure ratio and efficiency at the design point, and the mass flow rate at the design point decreases slightly.

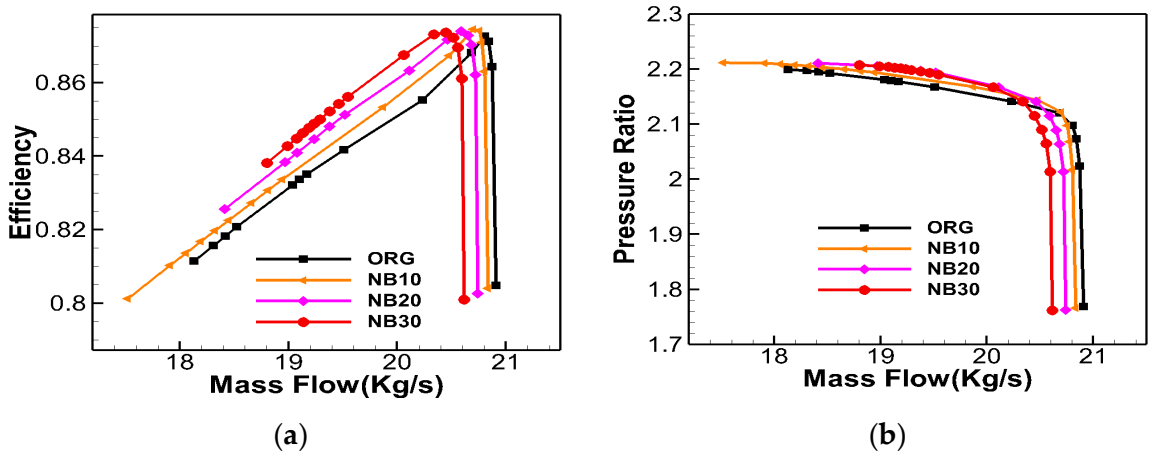

Figure 7. Comparison of isentropic efficiency and total pressure ratio of NB10, NB20, and NB30. (**a**) the isentropic efficiency. (**b**) the total pressure ratio.

Table 3. Comparison of design point performance and stall margin of NB10, NB20, and NB30.

Parameters	Mass Flow (kg/s)	Pressure Ratio	Efficiency (%)	Stall Margin
ORG	20.80	2.098	87.31	20.35%
NB10	20.70	2.122	87.48	20.71%
NB20	20.59	2.116	87.40	16.91%
NB30	20.45	2.115	87.37	13.52%

The efficiency of the design point of the tandem rotor with NB10 is increased by 0.37%, the stall margin of the rotor is increased, and the stall margin reaches 20.71%. With the increase of the negative bow angle, the stall margin of the tandem rotor gradually decreases, and the stall margin of the tandem rotor with NB30 decreases to 13.52%. From the comparison between the isentropic efficiency and the total pressure ratio characteristics, it can be seen that negative bow blades improve the efficiency and pressure ratio of the tandem rotor under all operating conditions, and improve the flow field structure of the tandem rotor. With the increase of the bow angle, the efficiency and total pressure ratio of the tandem rotor under the same mass flow conditions are improved more significantly.

Figure 8 shows the comparison of the spanwise distribution of the total pressure ratio and the efficiency of NB10, NB20, and NB30. Compared with ORG, negative bow blades significantly increase the efficiency and total pressure ratio of the rotor from a 20% span to a 85% span. With the increase of the bow angle, the increase in efficiency and total pressure ratio from a 20% to a 85% span is more significant. In addition, negative bow rotors deteriorate the flow field structure in the blade tip region, and at the same time, negative bow rotors also increase the total pressure loss of the hub end wall. With the increase of the bow angle, the total pressure loss in the blade tip region and the hub region gradually increases, and the decrease degree in the total pressure ratio also increases gradually.

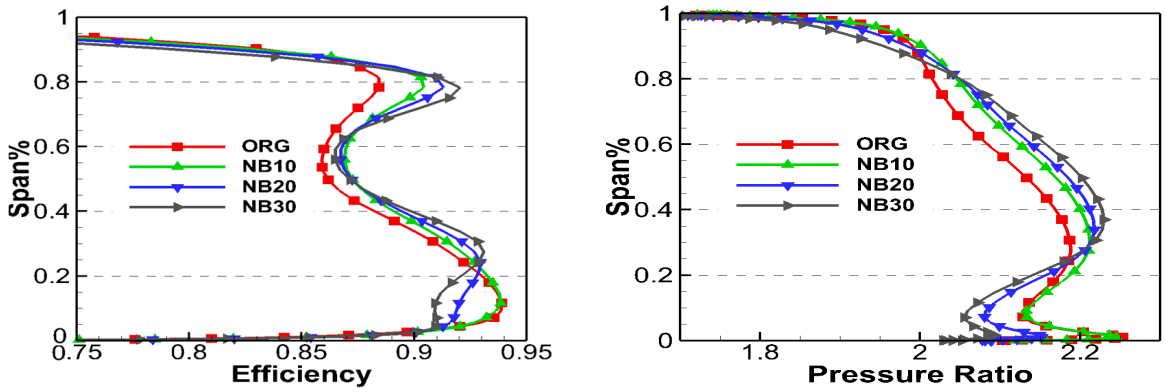

Figure 8. Comparison of the spanwise distribution of the total pressure ratio and the efficiency of NB10, NB20, and NB30. (**a**) the isentropic efficiency. (**b**) the total pressure ratio.

The negative bow blades increase the end wall loss of the case and hub, but improve the performance of most spans of the rotor blade. Therefore, the overall performance of the tandem rotor is improved, the average total pressure loss at the rotor outlet is reduced, and the average efficiency of the rotor is increased. This is consistent with the affect mechanism of negative bow blades on the flow field of the transonic single rotor. Previous studies have shown that negative bow blades generate pressure from the blade towards the upper and lower end wall by exerting radial force on the fluid in the blade channel. It is conducive to the migration of low-energy fluid near the middle of the blade to the end wall, which improves the flow field in the middle region of the blade span, and increases the blockage in the end wall. Therefore, the flow in middle span is improved, the efficiency in the middle span is increased, and the efficiency in the hub and case is decreased. However, the total pressure loss in the middle span of the original supersonic tandem rotor is larger and the efficiency is lower, so the three kinds of negative bow blades (NB10, NB20, and NB30) can obviously improve the flow field at the middle span of the blade.

Figure 9 shows the comparison of spanwise distribution of the inlet flow angle and the axial velocity density (AVD) of NB10, NB20, and NB30. Compared with ORG, the inlet flow angle of the tandem rotor with NB10 is reduced about 1° across the full span, and the flow moves along the direction of the negative incidence angle, resulting in a decrease of blade aerodynamic load across the full span. However, the total pressure at the rotor outlet increases because the efficiency of the middle region of the tandem rotor is improved. The tandem rotor with 20°and 30° negative bow increases the inlet flow angle in the hub region, resulting in an increment of blade aerodynamic load in this region. In addition, the inlet flow angle in the middle span is reduced by the tandem rotor with NB20, whereas the inlet flow angle in the middle span is basically unchanged by the tandem rotor with NB30. It can be seen from the AVD comparison diagram that the AVD in the hub and case is reduced by the three negative bow tandem rotors, whereas the AVD in middle span is increased. This is because the three negative bow tandem rotors migrate the low-energy fluid in middle span to the hub and case region, increase the amount of low-energy fluid in the hub and case region, and improve the flow field in the middle span.

Figure 10 shows the contrast diagram of surface static pressure distribution at different spans of NB10, NB20, and NB30. Compared with the ORG rotor, in the hub span region, the negative bow blades reduce the aerodynamic load on the leading edge and middle of the front blade, and also reduce the aerodynamic load on the middle of the rear blade. Therefore, the negative bow blades reduce the aerodynamic load on the hub region of tandem rotors, which is also illustrated in Figure 8b. In the middle span region, the negative bow blades increase the load on the front of the front blade and decrease the load on the front of the rear blade. The negative bow blades do not change the position of shock wave, but reduce the adverse pressure gradient behind the shock wave and the separation of

boundary layer behind the shock wave. In the tip span region, the negative bow blades reduce the aerodynamic load on the front and middle of the front blade, but have little influence on the aerodynamic load on the rear blade. Similar to the hub span region, the negative bow blades make the position of the shock wave moving forward to the front of the front blade, increase the Mach number of the wave and the inverse pressure gradient after the shock wave, and result in an increment of shock wave loss and the viscous loss of the boundary layer.

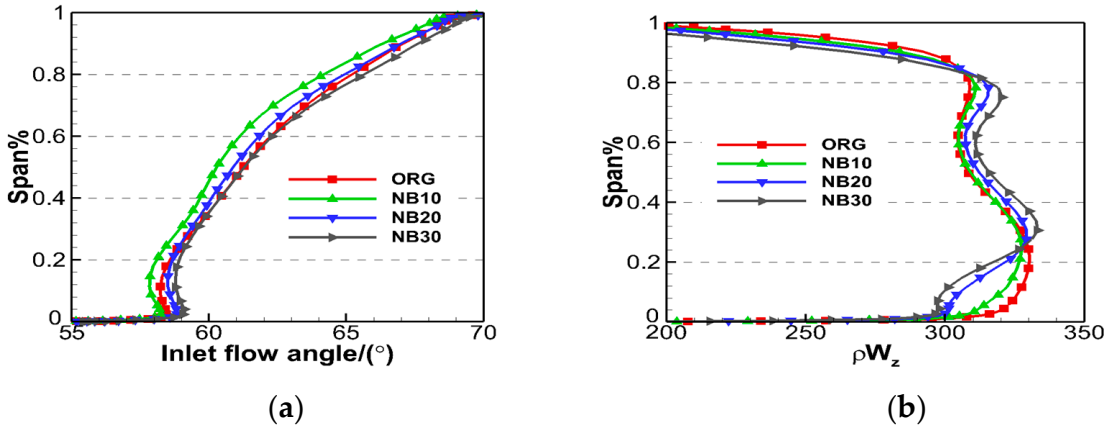

Figure 9. Comparison of spanwise distribution of the inlet flow angle and the axial velocity density (AVD) of NB10, NB20, and NB30. (**a**) the inlet flow angle. (**b**) the axial velocity density (AVD).

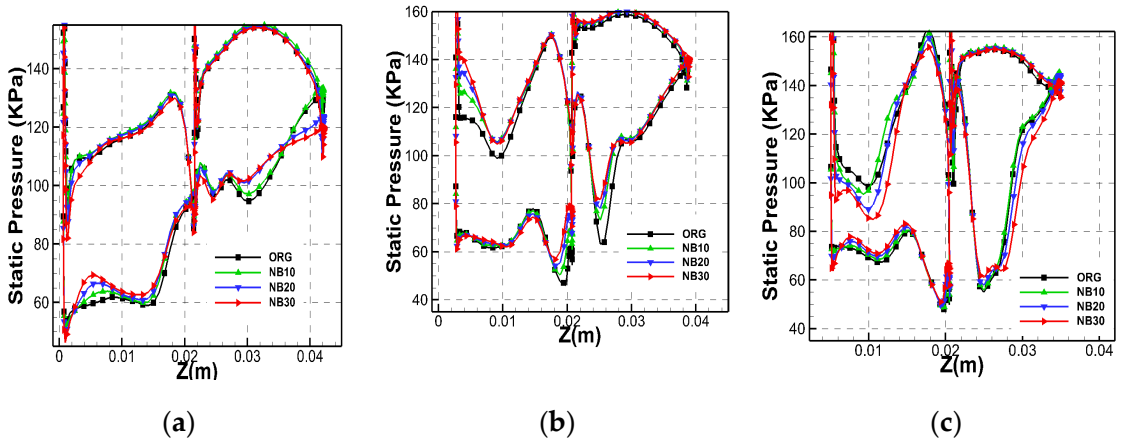

Figure 10. The contrast diagram of surface static pressure distribution at different spans of NB10, NB20, and NB30. (**a**) 10% span. (**b**) 50% span. (**c**) 90% span.

Figure 11 shows the comparison of static pressure and the limit flow line diagram on the suction surface of NB10, NB20, and NB30. There are obvious separation lines at the hub and middle of the suction surface of ORG, and the separation line extends from 10% to 60% of the blade spread. The separation line is generated by boundary layer separation caused by shock waves. The negative bow blades increase the boundary layer separation range in hub region of front blade, and the separation line caused by shock waves extends to the middle span. The range and intensity of the boundary layer separation in the hub region of the rear blade are also obviously increased. The negative bow blades reduce the radial migration range of low-energy fluid in the middle region of the rear blade. However, the radial migration intensity of low-energy fluid in the blade tip region was increased. With the increase of the bow angle, there is no obvious radial migration of low-energy fluid in the middle region, but a small range of corner separation region with high intensity appeared near the trailing edge of the blade tip, which increases the total pressure loss in the blade tip region.

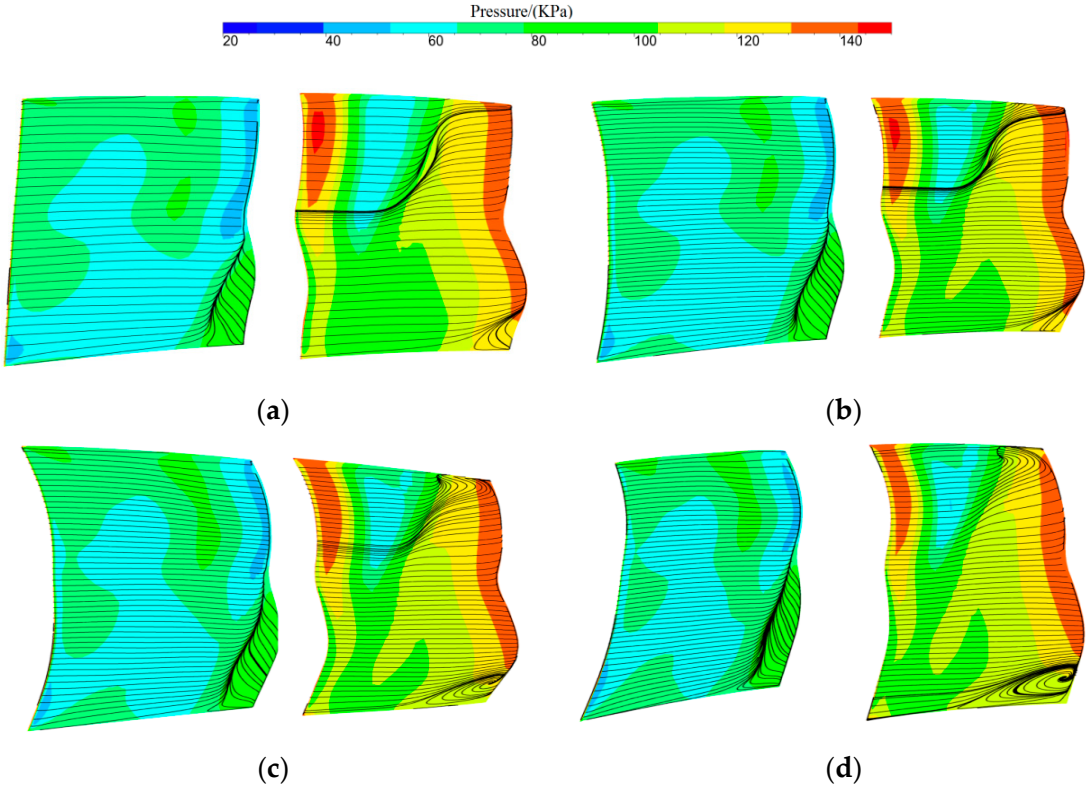

Figure 11. Comparison of static pressure and limit flow line diagram on suction s of NB10, NB20, and NB30. (**a**) ORG. (**b**) NB10. (**c**) NB20. (**d**) NB30.

Figure 12 shows the comparison of flow line and static pressure on the end-wall surface of the hub of NB10, NB20, and NB30. The flow field in the hub region is deteriorated due to the negative bow blades, and the deterioration degree increases with the increase of the bow angle. Firstly, the separation range and intensity of the boundary layer of the front blade and rear blade are increased due to the intersection of the suction surface branch of the horseshoe vortex at the leading edge of the blade and suction surface. When the negative bow angle is 30°, an obvious vortex zone is formed at the trailing edge of the rear blade. Secondly, the branch of the horseshoe vortex on the front blade pressure surface is mixed with the low-energy fluid separated from the corner region of the rear blade. According to past research, when the horseshoe vortex of the blade pressure surface develops downstream, it intertwines with the end wall boundary layer to form passage vortex. Therefore, the negative bow blades increase the mixing degree of the blade passage vortex and low energy fluid in the corner region, and further increase the deterioration degree of the flow field in the hub region.

Figure 13 shows the contrast diagram of the static pressure coefficient near the casing wall of NB10, NB20, and NB30. According to existing studies, the tip leakage vortex trajectory corresponds to the static pressure chute of the casing wall. Therefore, the static pressure isoline chute line near the casing end wall is used in this paper to approximate the trajectory of the tip leakage vortex, as shown by the red dotted line. It can be seen that the negative bow blade does not significantly change the initial position of the tip leakage flow in the front blade, but increases the intensity of the tip leakage flow. The circumferential deflection and axial length of the tip leakage flow of the front blade increase significantly, whereas the negative bow blade makes the tip leakage flow of the rear blade move to the trailing edge, reducing the intensity and influence range of the tip leakage flow of the rear blade. However, compared with the tip leakage flow of front blade, the intensity and range of the tip leakage flow of the rear blade are significantly smaller. Therefore, the negative bow blade increases the intensity of the tip leakage flow and deteriorates the flow field in the tip region.

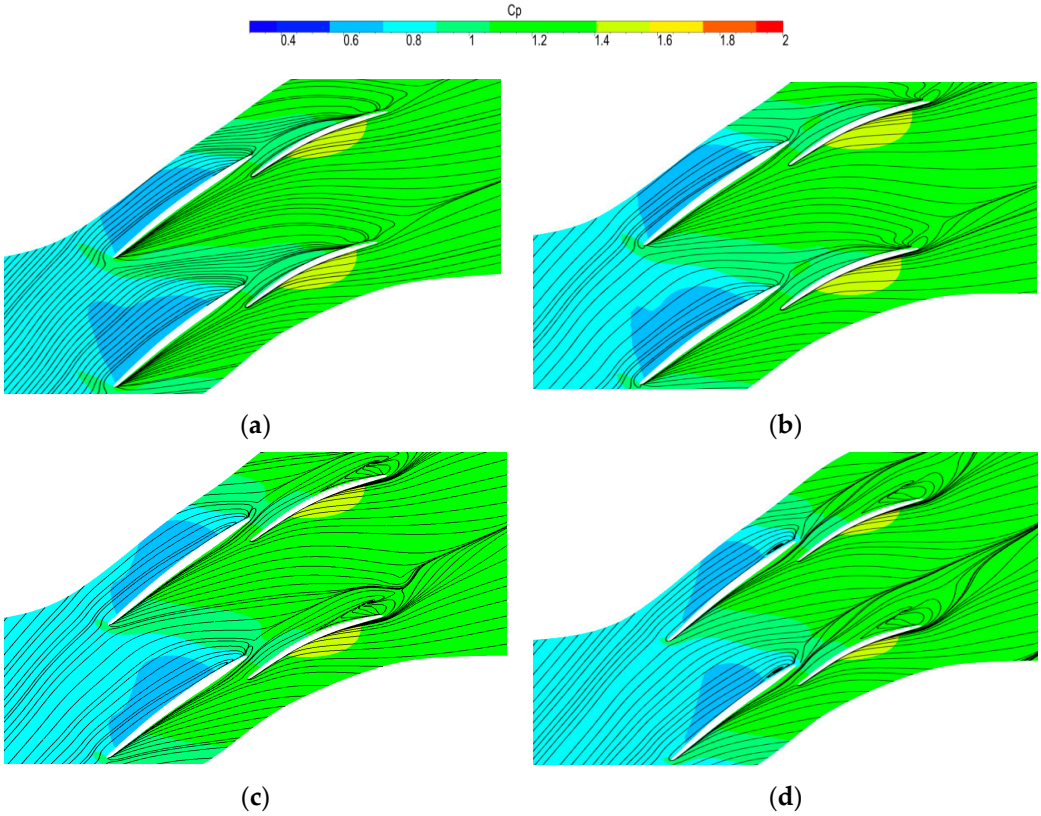

Figure 12. Comparison of flow line and static pressure diagram on the end-wall surface of the hub of NB10, NB20, and NB30. (**a**) ORG. (**b**) NB10. (**c**) NB20. (**d**) NB30.

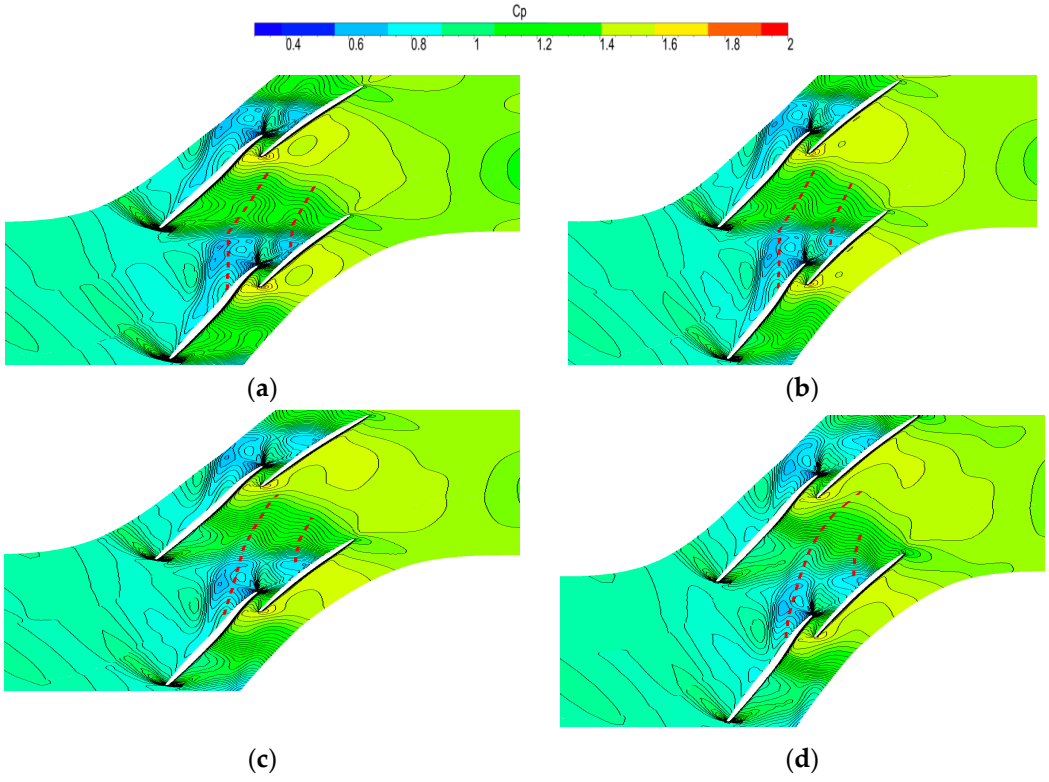

Figure 13. Contrast diagram of the static pressure coefficient near the casing wall of NB10, NB20, and NB30. (**a**) ORG. (**b**) NB10. (**c**) NB20. (**d**) NB30.

Figure 14 shows the comparison of the entropy diagram of the casing wall of NB10, NB20, and NB30. It can be seen that the negative bow blade worsens the flow field in the tip region and increases the total pressure loss in the tip region. As can be seen from the above analysis, this is because the negative bow blade pushes the low-energy fluid into in the tip region, which intensifies the blockage of the tip region passage and makes the shock wave in the tip region move towards the leading edge of blade. Therefore, the intensity of shock wave, the boundary layer separation, and the intensity of the tip leakage flow is increased.

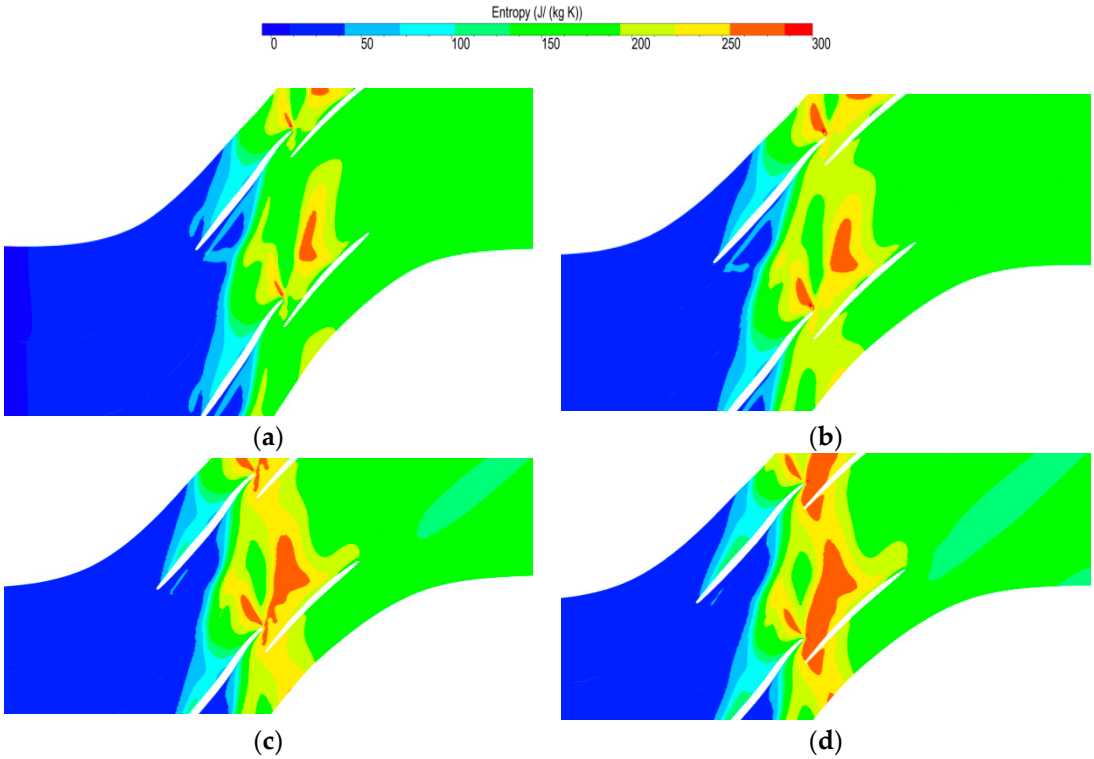

Figure 14. Comparison of the entropy diagram of the casing wall of NB10, NB20, and NB30. (**a**) ORG. (**b**) NB10. (**c**) NB20. (**d**) NB30.

4.2. Influence of a Positive Bow Blade on Supersonic Tandem Rotors

Figure 15 shows the comparison of isentropic efficiency and total pressure ratio characteristics of tandem rotors with different positive bow angles, including PB10, PB20, and PB30. Table 4 shows the comparison of design point performance and the stall margin of PB10, PB20, and PB30. It can be seen that, compared with the original rotor, the positive bow blade decreases the pressure ratio and efficiency at the design point and also reduces the stall margin of the tandem rotor. However, the positive bow blade increases the flow capacity of the tandem rotor. Compared with the ORG, the design point efficiency of the PB10 is reduced by 0.3%, the stall margin of the PB10 is reduced by 1%, and the design point flow rate of the PB10 is increased by 0.38%. With the increase of the angle, the effect of the positive bow on the column rotor is more remarkable.

Table 4. Comparison of design point performance and stall margin of PB10, PB20, and PB30.

Parameters	Mass Flow (kg/s)	Pressure Ratio	Efficiency (%)	Stall Margin
ORG	20.80	2.098	87.31	20.35%
PB10	20.88	2.074	87.05	19.35%
PB20	20.883	2.075	86.67	17.30%
PB30	20.90	2.052	86.22	15.22%

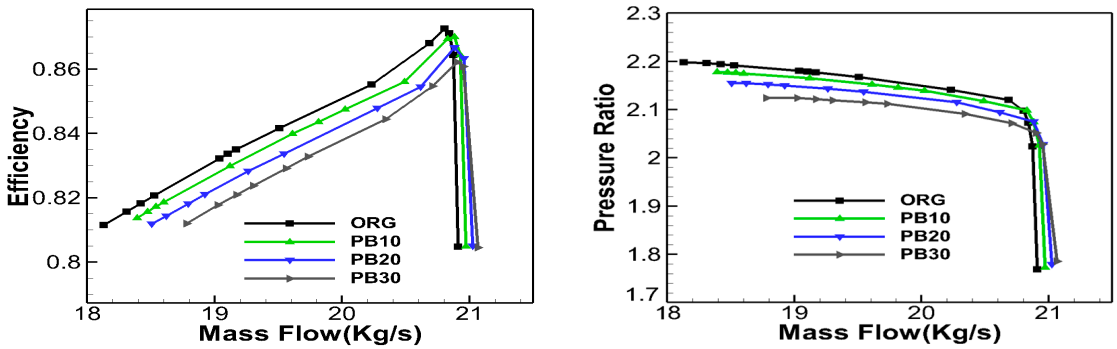

(**a**) (**b**)

Figure 15. Comparison of isentropic efficiency and total pressure ratio of PB10, PB20, and PB30. (**a**) the isentropic efficiency. (**b**) the total pressure ratio.

Figure 16 shows the comparison of efficiency and total pressure ratio spanwise distribution of PB10, PB20, and PB30. Compared with the ORG, positive bow blade reduces the efficiency from 10% to 50% of the span of the tandem rotors, but the efficiency of the hub region and the casing region is increased. In addition, the positive bow blade increases the total pressure ratio in the hub region and the casing region, but decreases the total pressure ratio in middle span of the tandem rotor. It is inconsistent with the variation of efficiency along the spanwise distribution. From Table 4, we can see that the positive bow blades decrease the maximum efficiency and worsen the flow field of the tandem rotor, which reduces the back pressure corresponding to the maximum efficiency point of the rotor. Therefore, the distribution of the total pressure ratio decreases significantly along the spanwise direction. In general, although the positive bow blade increases the efficiency of the end-wall region of the hub and casing, the overall performance of the tandem rotor is reduced because the flow field of the rotor with 10–50% blade span is deteriorated at the same time. This is consistent with the action mechanism of the positive bow blade on the flow field of the transonic single rotor.

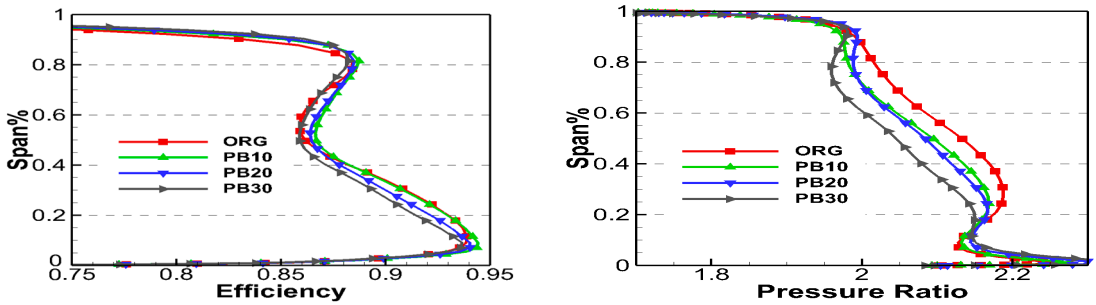

(**a**) (**b**)

Figure 16. Comparison of efficiency and total pressure ratio spanwise distribution. (**a**) the isentropic efficiency. (**b**) the total pressure ratio.

Past studies have shown that the positive bow blade exerts radial force on the fluid in the blade passage to generate pressure pointing from the end wall to the middle span, which is conducive to the migration of low-energy fluid in the hub and the casing region to the middle span and improves the flow field in the hub and the casing region. But at the same time, the efficiency of the positive bow blades is reduced. The total pressure loss in the middle span of the ORG is larger. Therefore, the positive bow blade further worsened the flow in the middle span. At the same time, the influence of the positive bow blade on the flow field of the supersonic tandem rotor has some different characteristics. The three positive bow blades do not deteriorate the performance at the high blade span

region, among which the positive bow blade with an angle of 10° and 20° can improve the performance of the tandem rotor from a 50% to a 80% span.

Figure 17 shows the comparison of spanwise distribution of the inlet flow angle and the axial velocity density (AVD) of PB10, PB20, and PB30. Compared with ORG, the positive bow blade reduces the inlet flow angle of the whole span of the tandem rotor, which makes the flow move along the direction of the negative incidence angle. In addition, the AVD in the hub and the casing region is increased and the low-energy fluid in the hub and the casing region is reduced by the three positive bow blades. At the same time, the positive bow blade also reduces the AVD in most spans of the tandem blades, and reduces the diffuser capacity of the corresponding span.

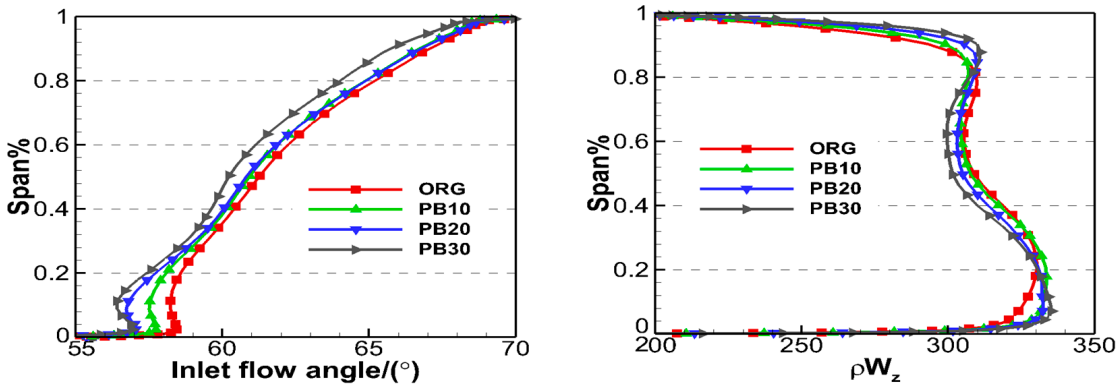

(**a**) (**b**)

Figure 17. Comparison of spanwise distribution of the inlet flow angle and the axial velocity density (AVD) of PB10, PB20, and PB30. (**a**) the inlet flow angle. (**b**) the axial velocity density (AVD).

Figure 18 shows the Comparison of surface static pressure distribution at different spans of PB10, PB20, and PB30. Compared with the ORG, the positive bow blade increases the aerodynamic load in the hub region and the tip region, and reduces the aerodynamic load in the middle span region. This is because the positive bow blade promotes the migration of the low-energy fluid in the hub region and the tip region to the middle span, reduces the low-energy fluid in the blade hub region and the tip region, and increases the diffusing capacity of the blade hub region and the tip region. In addition, in the blade hub region, the positive bow blade does not change the position of shock waves significantly, and the adverse pressure gradient after shock waves is basically unchanged. In the middle span, the positive bow blade obviously increases the adverse pressure gradient behind the shock wave of the front blade and the rear blade, and increases the separation loss of the boundary layer behind the shock wave. At the blade tip region, the positive bow blade migrates the position of the shock wave to the trailing edge, and meanwhile reduces the adverse pressure gradient behind the shock wave of the front blades. Therefore, the shock loss and separation loss of the boundary layer behind the shock wave is decreased.

Figure 19 shows the comparison of static pressure and the limit flow line diagram on the suction surface of PB10, PB20, and PB30. The positive bow blade increases the radial migration degree of low-energy fluid from the hub region to the middle span, and improves the flow field in the hub region. The positive bow blade has less influence on the corner separation range and strength of the hub region; this is why the corner separation range and strength of the rear blade are small. At the same time, the positive bow blade improves the flow field in the tip region of the rear blade and reduces the intensity of the radial migration of low-energy fluid in the middle span region. However, the positive bow blade worsens the flow field and increases the separation intensity of the boundary layer in the middle span.

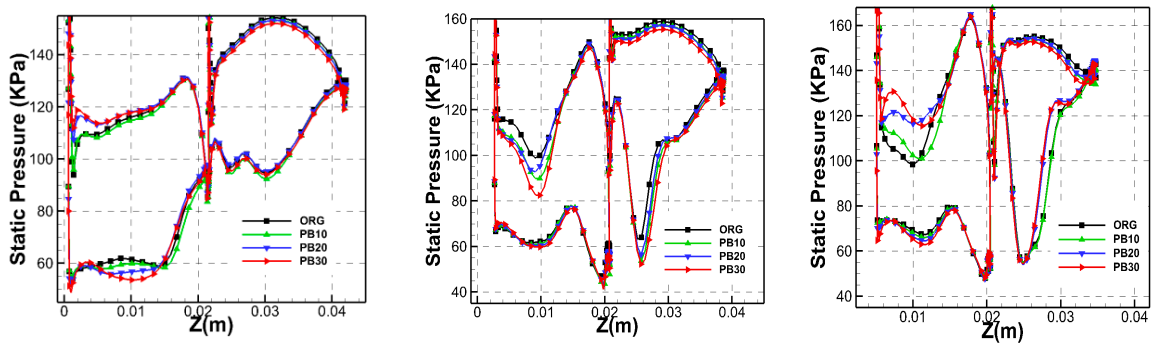

Figure 18. Comparison of surface static pressure at different spans of PB10, PB20, and PB30. (**a**) 10% span. (**b**) 50% span. (**c**) 90% span.

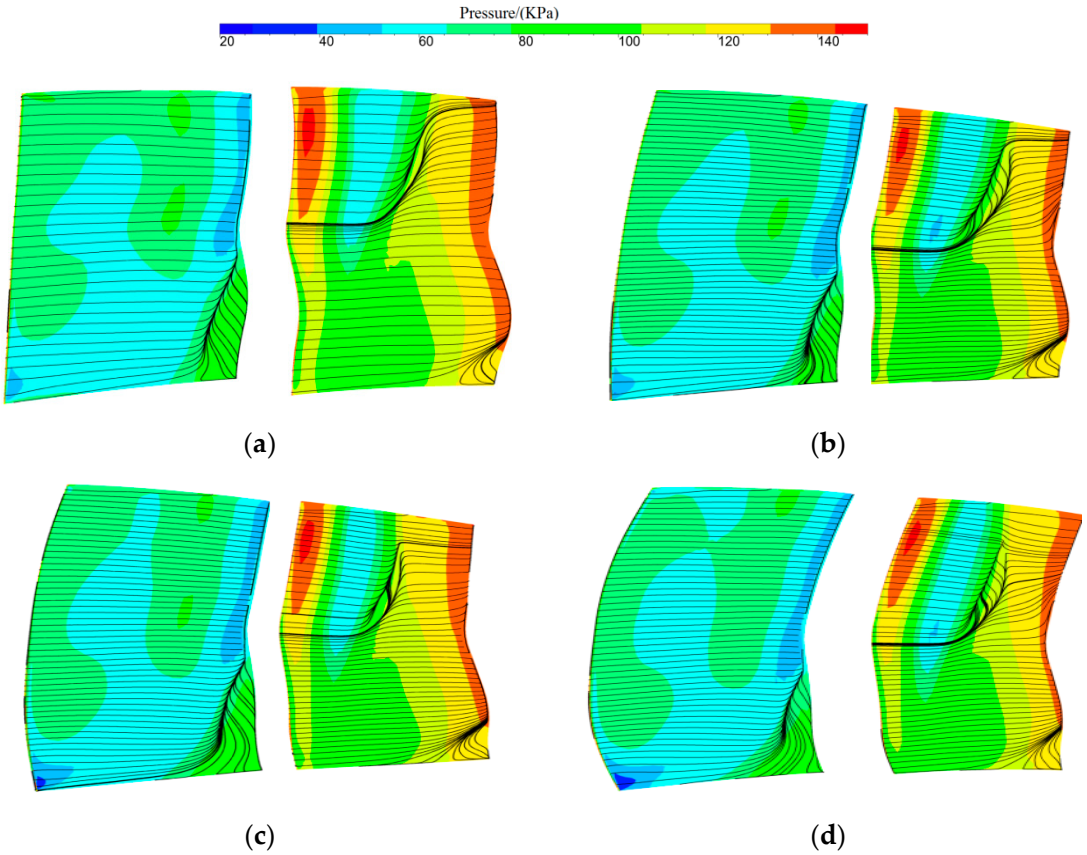

Figure 19. Comparison of static pressure and limit flow line diagram on suction surfaces of PB10, PB20, and PB30. (**a**) ORG. (**b**) PB10. (**c**) PB20. (**d**) PB30.

Figure 20 shows the comparison of flow line and the static pressure diagram on the hub end wall of PB10, PB20, and PB30. It can be seen that the positive bow blade improves the flow field in the hub region. With the increase of positive bow angle, the saddle point of the horseshoe vortex at the leading edge (the red circle point in Figure 20) gradually moves away from the leading edge of the blade to the middle blade passage. The intersection of the suction surface branch of the hoof vortex and the suction surface of the blade moves towards the leading edge of the blade. The intersection of the pressure surface branch of the horseshoe vortex and the suction surface of the blade also gradually moves towards the leading edge of the blade. This is because the positive bow blade improves the flow field in the hub region, the diffusing capacity of the hub region is increased, and the lateral and flow pressure gradients are significantly increased, which results in the saddle point

of the horseshoe vortex separation at the leading edge of the blade to move to the middle of the blade channel. At the same time, under the action of the large adverse pressure gradient, the pressure surface branch of the horseshoe vortex and the blade suction surface intersect earlier. It can be seen from the limiting streamline diagram of the suction surface that the lateral flow of the end wall is enhanced, and the flow field in the hub region is improved, but the separation range of the low-span boundary layer of the front rotor is slightly increased.

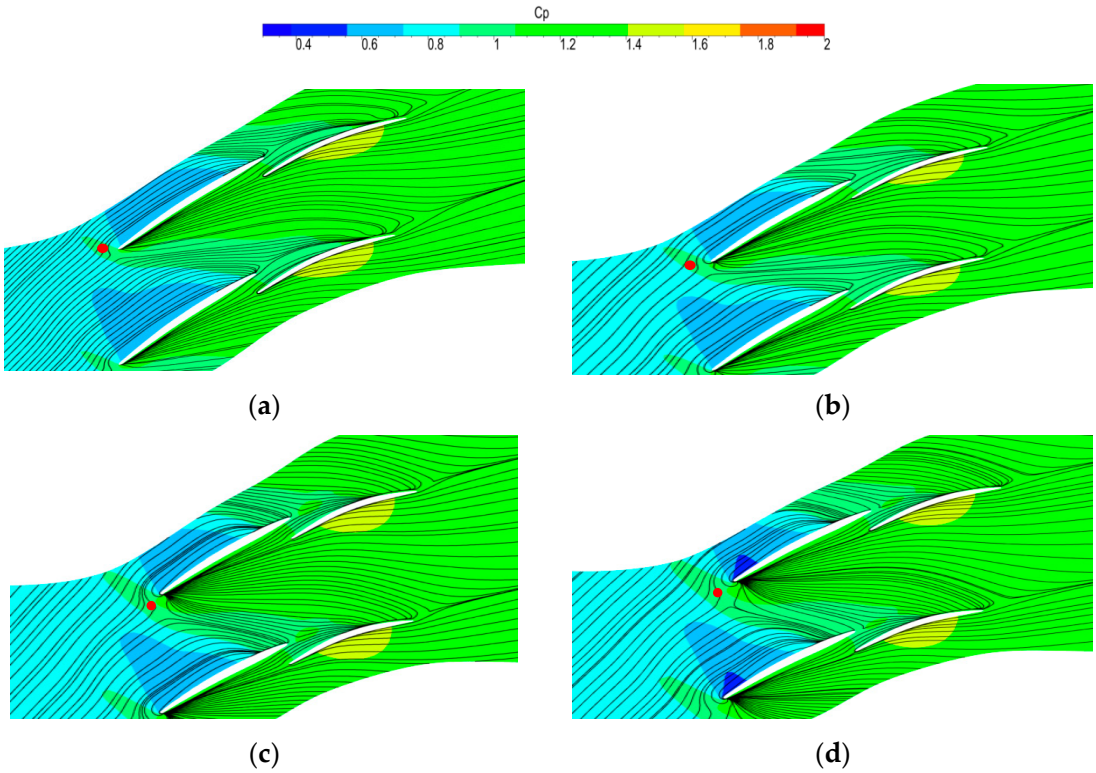

Figure 20. Comparison of flow line and static pressure diagram on the hub wall of PB10, PB20, and PB30. (**a**) ORG. (**b**) PB10. (**c**) PB20. (**d**) PB30.

Figure 21 shows the comparison of the static pressure coefficient diagram near the casing end wall of PB10, PB20, and PB30. This paper uses the static pressure contour line inclined groove connection near the casing end wall to approximate the blade. The trajectory of the tip leakage vortex is shown as the red dotted line in the figure. In this paper, the static pressure isoline inclined groove connection near the end wall of the casing is used to approximate the trajectory of the tip leakage vortex, as shown by the red dotted line in the figure. It can be seen that the positive bow blade does not significantly change the starting position of the tip leakage flow of the front and rear blades, but slightly increases the circumferential deflection of the tip leakage flow trajectory and increases the strength of the tip leakage flow.

Figure 22 shows the comparison of the entropy diagram of the casing wall of PB10, PB20, and PB30. The positive bow blade reduces the total pressure loss in the tip region. It can be seen from the previous analysis that this is because the positive bow blade promotes the movement of the low-energy fluid in the blade tip region to the low blade span, which increases the flow capacity of the blade tip channel and changes the shock wave structure in the blade tip region. The intensity of the shock wave and the range of the low-energy high-entropy fluid after the shock wave is also reduced.

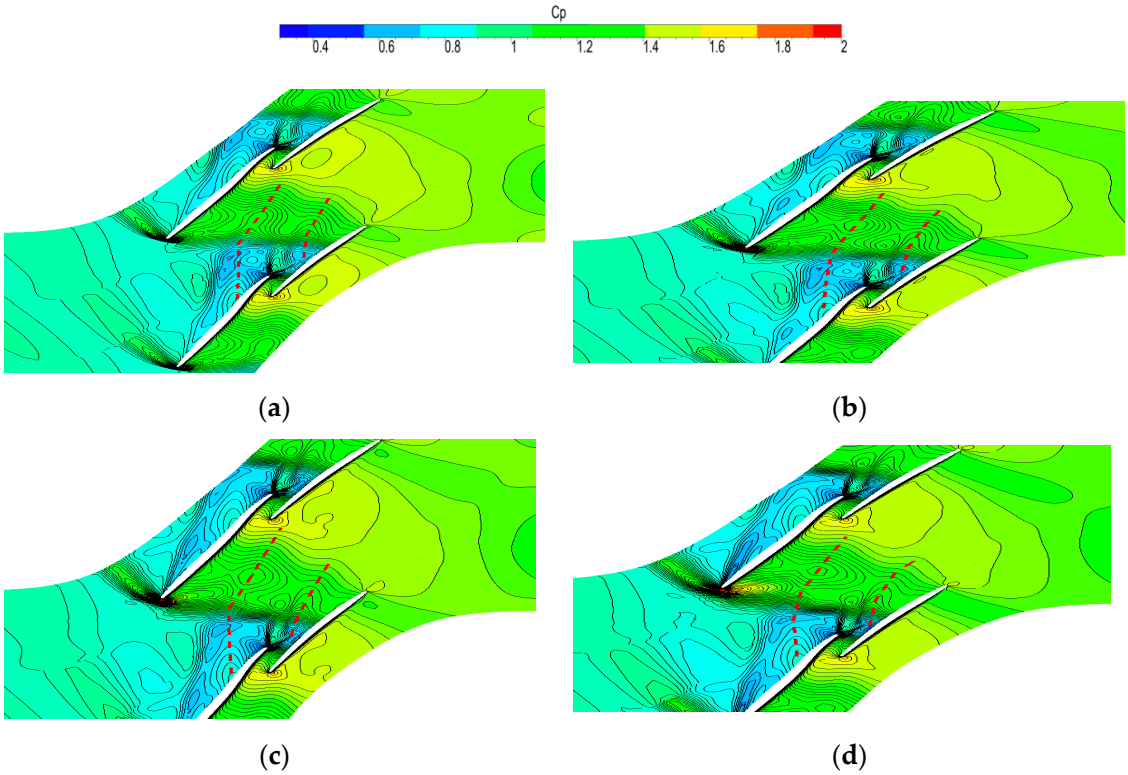

Figure 21. Comparison of the static pressure coefficient diagram near the casing end wall of PB10, PB20, and PB30. (**a**) ORG. (**b**) PB10. (**c**) PB20. (**d**) PB30.

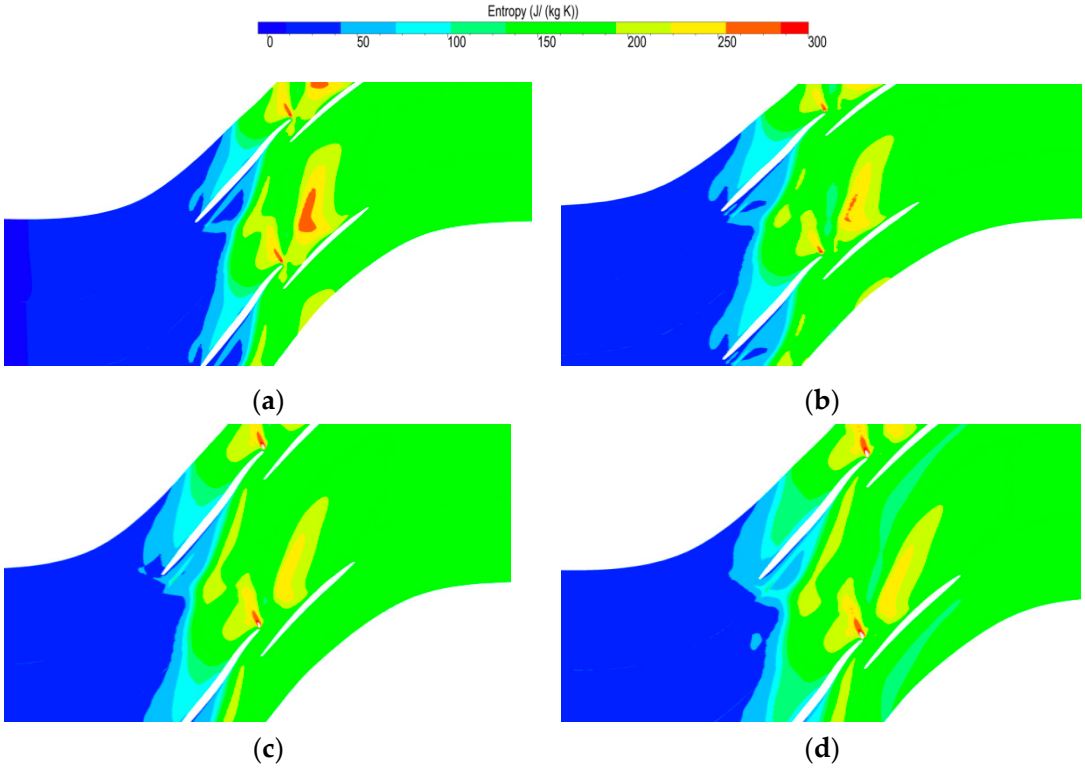

Figure 22. Comparison of the entropy diagram of the casing wall of PB10, PB20, and PB30. (**a**) ORG. (**b**) PB10. (**c**) PB20. (**d**) PB30.

5. Conclusions

In this study, in order to explore the influence mechanism of bow blades on the flow field of supersonic tandem rotors, the supersonic rotor rotor37 is taken as the prototype and redesigned to a supersonic tandem rotor. The main conclusions from the current research can be concluded as follows.

(1) Compared with the prototype rotor37, the efficiency of the tandem rotor is increased by 0.24% and the stall margin of the tandem rotor is increased by about 5.6% under the premise that the total pressure ratio is basically unchanged.

(2) Although the negative bow blade deteriorates the flow field in the tip region and the hub region, it significantly increases the efficiency and total pressure ratio of the tandem rotor from a 20% span to a 85% span. The efficiency of the design point of the tandem rotor with a negative bow angle of 10° is improved by 0.37%, and the stall margin is also increased to 20.71%. With the increase of the negative bow angle, the stall margin of the tandem rotor is gradually decreased, and the stall margin of the tandem rotor with a negative bow angle of 30° is decreased to 13.52%.

(3) Although positive bow blades improve the efficiency of the hub region and the casing region of tandem rotors, they significantly reduce the efficiency of the tandem rotor from 10% to 50%. The positive bow blade reduces the pressure ratio and efficiency at design point and reduces the stall margin of the tandem rotor, but increases the flow capacity of the tandem rotor. The design point efficiency of the tandem rotor with a positive bow angle of 10° is decreased by 0.3%, the stall margin is decreased by 1%, and the mass flow of the adesign point is increased by 0.38%.

Author Contributions: Conceptualization, B.L.; Data curation, Z.S.; Investigation, H.C. All authors have read and agreed to the published version of the manuscript.

Funding: This paper was funded by the Natural Science Foundation of China (no. 51676162).

Conflicts of Interest: The authors declare no conflict of interest.

References

1. Gummer, V.; Wenger, U.; Kau, H.P. Using sweep and dihedral to control three-dimensional flow in transonic stators of axial compressors. *J. Turbomach.* **2001**, *123*, 40–48. [CrossRef]
2. Gallimore, S.J.; Bolger, J.J.; Cumpsty, N.A.; Taylor, M.J.; Wright, P.I.; Place, J.M. The use of sweep and dihedral in multistage axial flow compressor blading—Part I: University research and methods development. *J. Turbomach.* **2002**, *124*, 521–532. [CrossRef]
3. Okui, H.; Verstraete, T.; Van den Braembussche, R.A.; Alsalihi, Z. Three-dimensional design and optimization of a transonic rotor in axial flow compressors. *J. Turbomach.* **2013**, *135*, 031009. [CrossRef]
4. Mao, X.C.; Liu, B.; Zhang, G.C.; Wu, X.X.; Deng, X.; Cheng, H. Effectiveness of Composite Optimization of Lean and Sweep on Transonic Compressor Performance. *J. Propuls. Technol.* **2015**, *36*, 996–1004.
5. Blaha, C.; Kablitz, S.; Hennecke, D.K.; Schmidt-Eisenlohr, U.; Pirker, K.; Haselhoff, S. Numerical investigation of the flow in an aft-swept transonic compressor rotor. In *Turbo Expo: Power for Land, Sea, and Air*; American Society of Mechanical Engineers: New York, NY, USA, 2000; Volume 78545, p. V001T03A060.
6. Denton, J.D.; Xu, L. The effects of lean and sweep on transonic fan performance. In *Turbo Expo: Power for Land, Sea, and Air*; American Society of Mechanical Engineers: New York, NY, USA, 2002; Volume 3610, pp. 23–32.
7. Wadia, A.R.; Szucs, P.N.; Crall, D.W.; Rabe, D.C. Forward swept rotor studies in multistage fans with inlet distortion. In *Turbo Expo: Power for Land, Sea, and Air*; American Society of Mechanical Engineers: New York, NY, USA, 2002; Volume 3610, pp. 11–21.
8. Bergner, J.R.; Kablitz, S.; Hennecke, D.K.; Passrucker, H.; Steinhardt, E. Influence of sweep on the 3D shock structure in an axial transonic compressor. In *Turbo Expo: Power for Land, Sea, and Air*; American Society of Mechanical Engineers: New York, NY, USA, 2005; Volume 47306, pp. 343–352.
9. Hah, C.; Wennerstrom, A.J. Three-dimensional flowfields inside a transonic compressor with swept blades. In *Turbo Expo: Power for Land, Sea, and Air*; American Society of Mechanical Engineers: New York, NY, USA, 1990; Volume 79047, p. V001T01A107.
10. Wadia, A.R.; Law, C.H. Low Aspect Ratio Transonic Rotors: Part 2-Influence of Location of Maximum Thickness on Transonic Compressor Performance. *J. Turbomach.* **1993**, *115*, 226–239. [CrossRef]
11. Cao, Z.; Zhang, X.; Liang, Y.; Liu, B. Influence of Blade Lean on Performance and Shock Wave/Tip Leakage Flow Interaction in a Transonic Compressor Rotor. *J. Appl. Fluid Mech.* **2022**, *15*, 153–167.
12. Razavi, S.R.; Sammak, S.; Boroomand, M. Multidisciplinary design and optimizations of swept and leaned transonic rotor. *J. Eng. Gas Turbines Power* **2017**, *139*, 122601. [CrossRef]

13. Bammert, K.; Staude, R. New features in the design of axial-flow compressors with tandem blades. In *Turbo Expo: Power for Land, Sea, and Air*; American Society of Mechanical Engineers: New York, NY, USA, 1981; Volume 79627, p. V002T08A012.
14. Bammert, K.; Staude, R. Optimization for rotor blades of tandem design for axial flow compressors. *ASME J. Eng. Power* **1980**, *102*, 369–375. [CrossRef]
15. Bammert, K.; Beelte, H. Investigations of an axial flow compressor with tandem cascades. *ASME J. Eng. Power* **1980**, *102*, 971–977. [CrossRef]
16. Wu, G.; Zhuang, B.; Guo, B. Experimental Investigations of Tandem Blade Cascades with Double Circular Arc Profiles. In *Turbo Expo: Power for Land, Sea, and Air*; ASME Paper, 85-IGT-94; American Society of Mechanical Engineers: New York, NY, USA, 1985.
17. Roy, B.; Saha, U.K. Experimental Analysis of Controlled Diffusion Compressor Cascades with Single and Tandem Airfoils. In *Turbo Expo: Power for Land, Sea, and Air*; ASME Paper, 95-CTP-41; American Society of Mechanical Engineers: New York, NY, USA, 1995.
18. Roy, B.; Saha, U.K. *On the Application of Variable Camber Blading in Axial Flow Fans and Compressors*; ASME Paper 96-TA-58; ASME: New York, NY, USA, 1996.
19. Urasek, D.C.; Janetzke, D.C. *Performance of Tandem-Bladed Transonic Compressor Rotor with Tip Speed of 1375 Feet per Second*; NASA TM X-2484; NASA: Greenbelt, MD, USA, 1972.
20. Hasegawa, H.; Matsuoka, A.; Suga, S. Development of highlyloaded fan with tandem cascade. In *41st Aerospace Sciences Meeting and Exhibit*; AIAA Paper 2003-1065; AIAA: Reston, VA, USA, 2003.
21. Sakai, Y.; Matsuoka, A.; Suga, S.; Hashimoto, H. *Design and Test of Transonic Compressor Rotor with Tandem Cascade*; The International Gas Turbine Congress: Tokyo, Japan, 2003.
22. McGlumphy, J.; Ng, W.F.; Wellborn, S.R. *Numerical Investigation of Tandem Airfoils Subsonic Axial-Flow Tan-Dem Compressor Blades*; ASME 2007-GT-43929; ASME: New York, NY, USA, 2007.
23. McGlumphy, J.; Ng, W.F.; Wellborn, S.R. *3D Numerical Investigation of Tandem Airfouls for a Core Compressor Rotor*; ASME 2008-GT-50427; ASME: New York, NY, USA, 2008.
24. Reid, L.; Moore, R.D. *Design and Overall Performance of Four Highly Loaded, High-Speed Inlet Stages for an Advanced High-Pressure-Ratio Core Compressor*; NASA-TP-1337; NASA: Greenbelt, MD, USA, 1978.
25. Suder, K.L.; Celestina, M.L. Experimental and Computational Investigation of the Tip Clearance Flow in a Transonic Axial Compressor Rotor. *J. Turbomach.* **1996**, *118*, 218–229. [CrossRef]